Photon-assisted capacitance–voltage study of organic metal–insulator–semiconductor capacitors

Watson, C.P.; Devynck, M.; Taylor, D.M.

Organic Electronics

DOI:
10.1016/j.orgel.2013.04.010

Published: 17/04/2013

Publisher's PDF, also known as Version of record

Organic Electronics 14 (2013) 1728–1736

Contents lists available at SciVerse ScienceDirect

Organic Electronics

journal homepage: www.elsevier.com/locate/orgel

Photon-assisted capacitance–voltage study of organic metal–insulator–semiconductor capacitors

Colin P. Watson, Mélanie Devynck, D.Martin Taylor *

School of Electronic Engineering, Bangor University, Dean Street, Bangor, Gwynedd LL57 1 UT, UK

ARTICLE INFO

Article history:
Received 30 January 2013
Received in revised form 22 March 2013
Accepted 3 April 2013
Available online 17 April 2013

Keywords:
Organic MIS device
Photocapacitance
C–V plot
Photoelectron yield
Geminate recombination
Poly(3-hexylthiophene)

ABSTRACT

The results are reported of a detailed investigation into the photoinduced changes that occur in the capacitance–voltage (*C–V*) response of an organic metal–insulator–semiconductor (MIS) capacitor based on the organic semiconductor poly(3-hexylthiophene), P3HT. During the forward voltage sweep, the device is driven into deep depletion but stabilizes at a voltage-independent minimum capacitance, C_{min}, whose value depends on photon energy, light intensity and voltage ramp rate. On reversing the voltage sweep, strong hysteresis is observed owing to a positive shift in the flatband voltage, V_{FB}, of the device. A theoretical quasi-static model is developed in which it is assumed that electrons photogenerated in the semiconductor depletion region escape geminate recombination following the Onsager model. These electrons then drift to the P3HT/insulator interface where they become deeply trapped thus effecting a positive shift in V_{FB}. By choosing appropriate values for the only disposable parameter in the model, an excellent fit is obtained to the experimental C_{min}, from which we extract values for the zero-field quantum yield of photoelectrons in P3HT that are of similar magnitude, 10^{-5} to 10^{-3}, to those previously deduced for π-conjugated polymers from photoconduction measurements. From the observed hysteresis we deduce that the interfacial electron trap density probably exceeds 10^{16} m^{-2}. Evidence is presented suggesting that the ratio of free to trapped electrons at the interface depends on the insulator used for fabricating the device.

1. Introduction

The capacitance–voltage (*C–V*) measurement, the so-called Terman method [1], has proved particularly useful for characterising the silicon/silicon dioxide interface in metal–oxide–semiconductor (MOS) technology. However, it has been recognized for many years that when applied to wide bandgap semiconductor materials the method is severely limited by the very low rate at which minority carriers are generated thermally – it may take years to generate thermally an inversion layer at the semiconductor–insulator interface. Consequently, during a *C–V* measurement on metal–insulator–semiconductor (MIS) capacitors based on wide bandgap materials, the inversion plateau is not observed. Rather, the capacitance continues to decrease as the device is driven into deep depletion. However, it has been shown that this limitation may be overcome in materials such as gallium nitride [2–5] and silicon carbide [6] by increasing the rate of minority carrier generation through optical stimulation with photons of energy greater than the semiconductor bandgap. Even sub-bandgap light has been used, in which case band-to-band generation of electron–hole pairs in the semiconductor is precluded so that carrier generation presumably occurred from trap states [7].

Not surprisingly, since organic semiconductors tend to have relatively large bandgaps, 2–3 eV, a similar limitation is encountered in *C–V* measurements on organic MIS capacitors [8–10]. *C–V* plots measured in the dark do not display the inversion plateau but continue to decrease monotonically as the applied voltage drives the device into

* Corresponding author. Tel.: +44 1248 382686; fax: +44 1248 361429.
E-mail address: d.m.taylor@bangor.ac.uk (D. Taylor).

1566-1199
http://dx.doi.org/10.1016/j.orgel.2013.04.010

deep depletion. For sufficiently high voltages and a sufficiently thin semiconductor, a minimum capacitance plateau will be observed eventually when the depletion region extends throughout the semiconductor. Under illumination, though, a minimum capacitance plateau is observed well before full depletion is attained while strong hysteresis occurs on the return voltage sweep. Subsequent *C–V* plots obtained in the dark exhibit a long-lived shift in flatband voltage, V_{FB}, indicative of deep trapping at the insulator–semiconductor interface. Similar hysteresis and shifts in V_{FB} are observed also in the transfer characteristics of organic thin film transistors (OTFTs) [11–13].

These effects occur when devices based on *p*-type materials are illuminated while biased into depletion, so that optically-induced free electrons escaping recombination drift to and become trapped at the semiconductor/insulator interface or in insulator states. Such trapping has been implicated in threshold voltage instability in OTFTs [14–16]. On the other hand, long-lived charge trapping may be used to realise charge storage memory transistors [17]. It is important, therefore, to develop methods for investigating and understanding the mechanisms causing these effects. The photon-assisted *C–V* measurement on MIS capacitors is such a method since it avoids the added complexity arising from orthogonal current flow through the accumulation channel of an OTFT and also the parasitic source-drain photocurrent when illuminated.

In the following, we report the results of a detailed investigation into the photocapacitance effect in solution-processed organic MIS capacitors based on poly(3-hexylthiophene), P3HT, as the semiconductor and UV-cured photoresist as the insulator. We also develop a quasi-static model which, although not complete, explains the main features observed experimentally. Interestingly, the model shows that a minimum capacitance plateau in the photocapacitance–voltage plot can arise simply from deep trapping at the semiconductor–insulator interface. At a particular trapping rate, the concomitant shift of the flatband voltage tracks the applied voltage sweep thus maintaining a constant capacitance without the need to invoke the presence of an inversion layer.

2. Experimental

MIS capacitors were formed on precleaned and dried indium tin oxide (ITO) coated glass slides to act as a common gate electrode. The insulating layer was prepared from SU8 2000.5 photoresist (Microchem Ltd.) diluted in the ratio 50:50 (v/v) in cyclopentanone and filtered through 0.2 μm PTFE filters. Spin-coating in a nitrogen atmosphere at a final speed of 2000 rpm, pre-curing at 95 °C for 1 min, followed by UV curing (in air) and a post-cure bake at 95 °C for 1 min and 200 °C for 30 min under nitrogen, yielded a smooth, uniform 194 nm thick film. Regio-regular poly(3-hexylthiophene), P3HT, from Sigma Aldrich was prepared as a 1% solution in anhydrous chloroform, filtered and spin-cast again under nitrogen onto the SU8 layer at 3000 rpm for 1 min then dried in a vacuum oven at 90 °C for 1 h yielding films ~100 nm thick film. The devices were completed by thermally evaporating a 50 nm gold film through a shadow mask to form an array of 2 mm diameter circular contacts. Completed devices were placed in a bespoke sample holder and mounted in a cryostat (Oxford Instruments Optistat Model DN-V) located in a darkroom to eliminate the effects of stray light.

The optical experiments were undertaken over the range 400–700 nm using a xenon discharge lamp coupled to a monochromator (Jobin Yvon Triax 320). Monochromatic light was transmitted into the cryostat through a quartz window and illuminated the devices through the ITO contact (Fig. 1a). Since the main effects are expected to be associated with the insulator/semiconductor interface this arrangement minimized the 'internal filter' effect that would otherwise arise from absorption in the P3HT film [8] when illuminated through the upper electrode. The power of the light incident on the devices was measured using a sensor (Anritsu model MA9411A1) and power meter (Anritsu modelM-9001A) and could be set approximately by adjusting the exit slit of the monochromator.

C–V plots and admittance spectra (capacitance–frequency, *C–f* and conductance–frequency, *G–f*) were

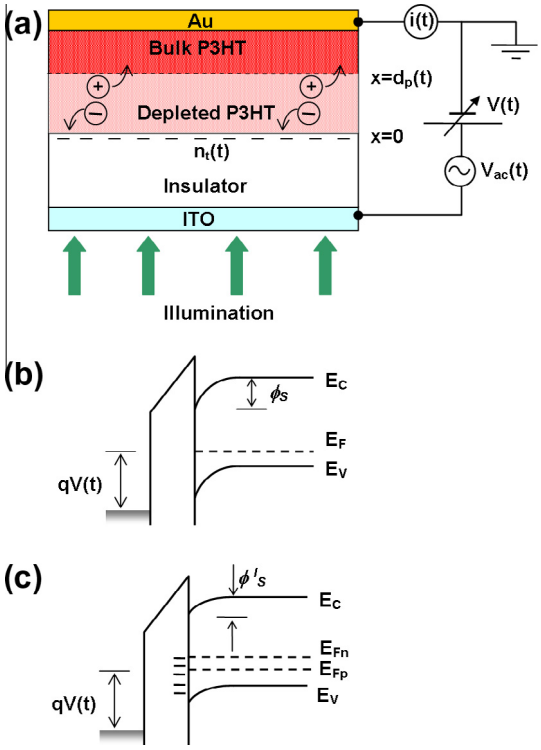

Fig. 1. (a) Diagram showing the measurement concept. Device capacitance is computed in the LCR meter from the ratio of the small signal current, $i(t)$ to the small signal voltage, $v_{ac}(t)$ while the applied bias, $V(t)$, sweeps the MIS capacitor from accumulation to depletion and back. Light enters the device through the ITO back contact and generates excitons in the P3HT depletion region which dissociate, releasing free electrons to become trapped at the interface. Also shown are classic band diagrams for a MIS capacitor based on a *p*-type semiconductor in quasi-steady state, (b) in the dark and (c) under illumination. In the latter case, illumination substantially increases the minority electron concentration thus splitting the hole and electron quasi Fermi levels, E_{Fp} and E_{Fn} respectively. Electrons occupy interface states up to E_{Fn}, their screening effect reducing the semiconductor surface potential from ϕ_S to ϕ_S^l.

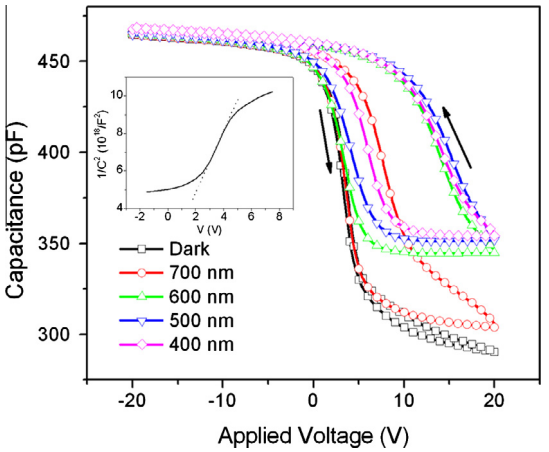

Fig. 2. *C–V* plots showing the effect of changing the wavelength of the incident light. The plots were obtained at a scan rate of 0.2 V/s. The light intensity in each case was 400 nm: 1.92 W/m^2 (3.86×10^{18} photons/m^2 s); 500 nm: 1.86 (4.68×10^{18}); 600 nm: 1.85 (5.58×10^{18}) and 700 nm: 1.03 (3.77×10^{18}). The inset shows the dark data obtained in the forward sweep re-plotted in Mott-Schottky format.

obtained with an Agilent 4284A Precision LCR Meter. The signal amplitude was 100 mV in all cases. For *C–V* measurements the signal frequency was 1 kHz.

Prior to each measurement, devices were short-circuited at room-temperature for 10 min to remove residual effects from previous measurements. When necessary, the devices were thermally annealed in order to return them to their initial state. Sample temperature was controlled using a model ITC502 temperature controller (Oxford Instruments).

3. Experimental results

3.1. Dark measurements

Prior to undertaking photon-assisted *C–V* measurements, admittance spectra were obtained over the range

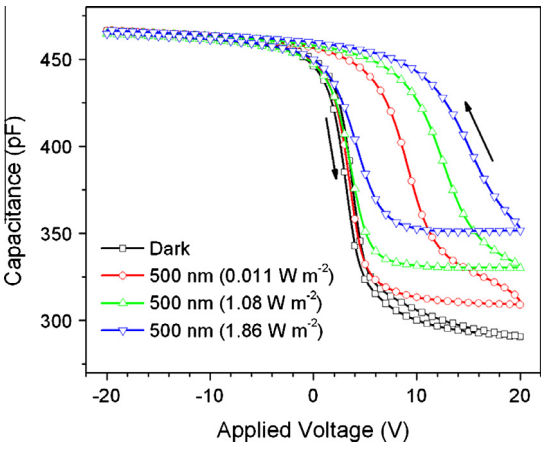

Fig. 3. *C–V* plots obtained during illumination with 500 nm light showing the effect of increasing light intensity. The voltage ramp rate was 0.2 V/s.

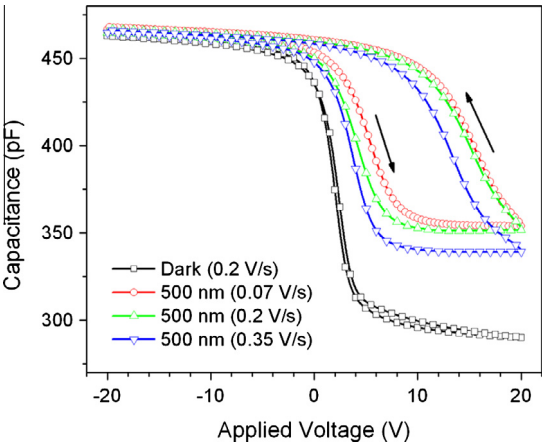

Fig. 4. *C–V* plots obtained during illumination with 500 nm light showing the effect of increasing the voltage sweep rate. The light intensity was 1.86 W/m^2.

100 Hz to 1 MHz for all our devices. The results were similar to those reported previously (e.g. Fig. 4, Ref. [18]). Although the insulator here is different, the effects related to the P3HT film were identical. At low frequencies and when driven into depletion, the device capacitance decreased from a value corresponding to the insulator capacitance to one commensurate with the voltage-independent capacitance measured at high frequency. The latter value corresponded to the series sum of the insulator and semiconductor capacitances. The bulk hole mobility in P3HT is low so that, above some critical frequency, carriers are unable to follow the signal frequency leading to the so-called Maxwell-Wagner dispersion for a two-layer capacitor. The corresponding relaxation frequency marks the transition from low to high frequency behaviour and occurred at ~10 kHz in our devices, but shifted slightly to higher frequencies as the P3HT depleted. Taken together with the linear Mott-Schottky plot in the inset of Fig. 2, these observations provide unequivocal evidence for the formation of a classic depletion region of ionized acceptor dopants in the P3HT [18] in keeping with previous reports for P3HT [19–21]. These preliminary experiments also demonstrated the need to undertake *C–V* measurements at frequencies well below 10 kHz in order to obtain meaningful results.

In Fig. 2 is shown a typical *C–V* plot obtained at a voltage scan rate of 0.2 V/s with the device in the dark. Both the forward and reverse voltage sweeps traced virtually identical paths. For increasingly positive voltages, the capacitance decreased from 470 pF, the insulator capacitance, down to ~290 pF corresponding to full depletion. Since a classic space-charge region forms in the P3HT, the data was re-plotted (inset Fig. 2) in Mott-Schottky format, i.e. as C^{-2} vs V, [22] the linear slope yielding a doping density, N_A, ~3×10^{22} m^{-3} and similar, therefore, to values we have reported previously for the same grade of P3HT [18,23,24] and that others have also reported for P3HT [19–21]. The origin of the dopants is likely to be oxidative and/or photo-oxidative products of polythiophene resulting from exposure to atmospheric oxygen or ozone [20,21,25,26].

3.2. Effect of photon energy

Also shown in Fig. 2 are C–V plots obtained when illuminating the same device with photons of four different wavelengths in the range 400–700 nm. As for the dark measurement, the voltage scan rate was maintained at 0.2 V/s in all cases. For measurements under illumination, we note that the photon flux density, ϕ_0, arriving at the sample is related to the incident light power, I_0, through the relation

$$\phi_0 = \frac{\lambda I_0}{hc} \tag{1}$$

where λ is the wavelength, h Planck's constant and c the speed of light. Owing to the non-uniform spectral output of the xenon lamp, the intensity at different wavelengths was adjusted in an effort to achieve constant ϕ_0. In the event, ϕ_0 varied from 3.77×10^{18} to 5.58×10^{18} photons/m^2 (see caption to Fig. 2) for the wavelengths investigated.

As seen in Fig. 2, the effect of illuminating with 700 nm light was minimal. On the forward sweep, the C–V plot followed that obtained in the dark until a minimum capacitance plateau, C_{min}, was reached at a slightly higher value than that corresponding to full depletion. On the return sweep, however, counter-clockwise hysteresis occurred, consistent with a long-lived positive shift in V_{FB}. When illuminated with photons in the range 600–400 nm, the C_{min} plateau was attained much earlier in the forward sweep. The width of the hysteresis loop at half height also changed, increasing to ~10 V between 600 and 500 nm, but then decreasing to ~7.5 V at 400 nm.

We note, then, that the effects of illumination are greatest for wavelengths below the absorption threshold for P3HT, ~650 nm, and peak at wavelengths corresponding to maximum absorption, ~500 nm. These results are consistent, therefore, with the photogeneration of electron–hole pairs in the P3HT. The small effect observed at 700 nm suggests that, in this case, carrier generation may occur as a result of excitation out of tail states as reported in [7].

The counter-clockwise hysteresis observed during illumination is related to deep trapping of electrons at the P3HT/SU8 interface. The positive shift, ΔV_{FB}, in the flatband voltage is related to n_t, the effective density of photoinduced electrons trapped at the interface through the relation [27]

$$\Delta V_{FB} = \frac{q n_t}{C_i}. \tag{2}$$

Here q is the electronic charge and $C_i = 1.48 \times 10^{-4}$ F m^{-2} the capacitance per unit area of the insulator. For $\Delta V_{FB} = 10$ V, the density of trapped electrons, $n_t = 9 \times 10^{15}$ m^{-2} suggesting that the total density of interface traps may be even greater.

3.3. Effect of incident power

In Fig. 3 we shows the effect of increasing the incident power from 0.011 to 1.86 W/m^2 while illuminating with 500 nm photons and maintaining a constant voltage sweep rate of 0.2 V/s. At low incident power during the forward voltage sweep, the C–V plot tracked closely the dark plot. Just before full depletion the capacitance eventually stabilized at a slightly higher minimum capacitance. On the reverse sweep moderate hysteresis was observed. Upon increasing the incident power, a clear trend of increasing C_{min} and increasing hysteresis width occurred, reflecting the increasing photon dose absorbed in the P3HT. The maximum shifts observed in the flatband voltage were again consistent with a minimum interfacial electron trap density of $\sim 10^{16}$ m^{-2}.

3.4. Effect of voltage sweep rate

Fig. 4 shows the effect of changing the voltage sweep rate from 0.07 to 0.35 V/s while illuminating with 500 nm photons at an intensity of 1.86 W/m^2. Again the photocapacitance plots showed trends reflecting an increase in the incident photon dose – both C_{min} and the width of the hysteresis loop increased as the voltage sweep rate decreased.

4. Theoretical model

In this section we develop a model that explains the main features of the experimental results presented above. The key features are illustrated in Fig. 1a which shows an ideal MIS capacitor biased into depletion being illuminated through the transparent ITO electrode. Photons absorbed in the P3HT generate bound electron–hole pairs (excitons) which dissociate in the electric field of the depletion region releasing holes into the bulk semiconductor, while electrons drift to and become trapped at the P3HT/SU8 interface. The width, $d_p(t)$, of the depletion region is determined by the applied voltage, $V(t)$, and by changes in the flatband voltage, $V_{FB}(t)$, occurring as a result of interfacial electron trapping.

Although applying classical semiconductor band models to polymeric semiconductors is debatable, nevertheless, they can prove useful in aiding the understanding of the processes occurring in experiments such as those reported here. In Fig. 1b we show the band diagram of a p-type semiconductor in quasi steady-state during a C–V sweep. The applied voltage causes band-bending ϕ_S in the semiconductor depletion region. The concentration of thermally generated electrons is extremely low and little or no interfacial trapping occurs. We contrast this with the situation under illumination in Fig. 1c where the electron concentration is increased sufficiently to split the electron quasi Fermi level, E_{Fn}, from the hole quasi Fermi level E_{Fp} [28]. This increased concentration of electrons now allows the filling of interfacial electron traps up to E_{Fn}. The resultant screening effect causes a shift ΔV_{FB} in the flat-band voltage (Eq. (2)) and a reduction in band-bending to ϕ'_S.

To provide a framework within which to develop the model, the following assumptions were made.

(i) A linear voltage ramp $V(t) = \gamma t$ is applied to the ITO electrode during the period $0 \leqslant t \leqslant t_f$, which reaches a final value V_f at time $t = t_f$. At the end of this forward sweep, the voltage ramp is reversed so that $V(t) = [V_f - \gamma(t - t_f)]$ for $t > t_f$.

(ii) Noting that the depletion region behaves as a parallel plate capacitor with plate separation equal to $d_p(t)$ [27], the measured device capacitance per unit area, $C(t)$, is the series sum of the insulator and depletion capacitances and evaluated from the expression [22,27]

$$\frac{1}{C(t)} = \frac{1}{C_i} + \frac{d_p(t)}{\varepsilon\varepsilon_0}. \tag{3}$$

(iii) Light enters the capacitor through the insulator (Fig. 1) and is absorbed in the P3HT film following Lambert's law i.e. the intensity, $I(x)$, of light of wavelength, λ, and initial intensity, I_0, having traversed a distance x into a material with a characteristic absorption coefficient $\alpha(\lambda)$ is given by

$$I(x) = I_0 e^{-\alpha(\lambda)x}. \tag{4}$$

(iv) The rate at which the incident light generates excitons locally in the P3HT film is determined by the local change in photon density i.e.

$$\frac{dN_{ex}(x)}{dt} = -\eta\frac{d\phi(x)}{dx} = \eta\frac{\lambda}{hc}\alpha(\lambda)I_0 e^{-\alpha(\lambda)x} \tag{5}$$

where η represents the efficiency of exciton generation, $N_{ex}(x)$ the exciton concentration and $\phi(x)$ the photon flux density at position x.

(v) We assume that excitons dissociate into free charge carriers subject to the local Coulomb and electric fields following the Onsager model for geminate recombination [29]. Although derived initially for electrolyte solutions, it has been applied widely to a range of experimental conditions and materials, for example, the photoconductive yield in anthracene [30] and amorphous selenium [31], for X-ray induced conductivity in polyvinyl-*n*-carbazole [32] and for electron-beam induced conductivity in SiO_2 [33]. Thus, for low to moderate electric fields, F, the probability, $\xi(F)$, that excitons dissociate into free carriers may be written as

$$\xi(F) = \xi(0)\left(1 + \frac{e^3}{8\pi\varepsilon\varepsilon_0 k^2 T^2}F\right) \tag{6}$$

where $\xi(0)$ is the probability of dissociation when $F = 0$, ε the relative permittivity, ε_0 the permittivity of free space, k is Boltzmann's constant and T the absolute temperature. At higher electric fields, $\xi(F)$ saturates due to the presence of higher order terms which are ignored in Eq. (6). Barth and Bässler [34] report that, in the electric field range 10^7–10^8 V/m, the quantum yield in polyparaphenylene vinylene-ether (PPV-ether) increased superlinearly with electric field, which nevertheless could be fitted by a modified Onsager model [35]. Here, as a first approximation, we continue with the linear field-dependence in Eq. (6).

(vi) Solving Poisson's equation for a depletion region composed of a uniform density, N_A, of ionized acceptors, subject to the boundary condition that $F = 0$ in the bulk semiconductor, shows that the local electric field, $F(x)$, within the depletion region increases linearly from 0 at the depletion edge ($x = d_p(t)$) to a maximum value at the semiconductor/insulator interface ($x = 0$) following the equation [22,27]:

$$F(x) = \frac{qN_A}{\varepsilon\varepsilon_0}(d_p(t) - x). \tag{7}$$

(vii) Free holes escaping geminate recombination in the depletion region drift into the P3HT bulk while free electrons drift to the P3HT/SU8 interface where we assume they are all trapped causing both $V_{FB}(t)$ and $d_p(t)$ to change with time. Consequently, the rate of electron trapping at the interface per unit area is given by

$$\frac{dn_t(t)}{dt} = \eta\frac{\lambda I_0}{hc}\xi(0)\alpha(\lambda)\int_0^{d_p(t)} e^{-\alpha(\lambda)x}(1 + \beta F(x))dx \tag{8}$$

where

$$\beta = \frac{e^3}{8\pi\varepsilon\varepsilon_0 k^2 T^2}. \tag{9}$$

Integration of Eq. (8) then yields

$$\frac{dn_t(t)}{dt} = K\frac{qN_A}{\varepsilon\varepsilon_0} \times \left[d_p(t) + \left(\frac{\varepsilon\varepsilon_0}{\beta qN_A} - \frac{1}{\alpha(\lambda)}\right)\left(1 - e^{-\alpha(\lambda)d_p(t)}\right)\right] \tag{10}$$

with

$$K = \eta\xi(0)\beta\frac{\lambda I_0}{hc}. \tag{11}$$

Values for the absorption coefficient, $\alpha(\lambda)$, calculated from n–k data obtained from spectroscopic ellipsometry measurements made on our P3HT films are given in Table 1, from which we see that $\alpha(\lambda)^{-1}$ must be $\geqslant 1.3 \times 10^{-7}$ m. For experimentally relevant values of $T = 293$ K, $\varepsilon = 3$ and $N_A = 3 \times 10^{22}$ m^{-3}, then $\beta = 3.75 \times 10^{-7}$ m/V so that $\varepsilon\varepsilon_0/\beta qN_A = 1.48 \times 10^{-8}$ m, which is much smaller than $\alpha(\lambda)^{-1}$. Therefore, Eq. (8) may be simplified, to

$$\frac{dn_t(t)}{dt} = K\frac{qN_A}{\varepsilon\varepsilon_0}\left[d_{p(t)} - \frac{1}{\alpha(\lambda)}\left(1 - e^{-\alpha(\lambda)d_p(t)}\right)\right]. \tag{12}$$

(viii) From standard MIS capacitor theory [22,27], the resulting shift in flatband voltage $V_{FB}(t)$ is given by

$$V_{FB}(t) = \frac{q}{C_i}n_t(t) = \frac{q}{C_i}\int_0^t \frac{dn_t(t)}{dt}dt \tag{13}$$

and the instantaneous width of the depletion region, $d_p(t)$, by [27]

$$d_p(t) = \frac{\varepsilon\varepsilon_0}{C_i}\left(\sqrt{1 + \frac{2C_i^2}{\varepsilon\varepsilon_0 qN_A}(V(t) - V_{FB}(t))} - 1\right). \tag{14}$$

5. Simulation results

The equations developed in the previous section were entered into a MATLAB® program to generate C–V plots as a function of ramp rate and illumination conditions.

Table 1
Material constants used in the simulations. Values for the absorption coefficient, $\alpha(\lambda)$, were calculated from *n-k* data obtained from spectroscopic ellipsometry measurements on our P3HT films undertaken by Dr. T. Jenkins, Aberystwyth University, UK.

N_A (m^{-3})	C_i (F/m^2)	d_{P3HT} (nm)	ε	$\alpha(700)$ (m^{-1})	$\alpha(600)$ (m^{-1})	$\alpha(500)$ (m^{-1})	$\alpha(400)$ (m^{-1})
3×10^{22}	1.48×10^{-4}	106	3	8.2×10^5	7.2×10^6	7.7×10^6	2.3×10^6

The material constants used in the calculations are given in Table 1. C_i was deduced from the accumulation capacitance measured in *C–V* and *C–f* plots obtained in the dark at 1 kHz. The thickness, d_{P3HT}, of the P3HT film was deduced assuming that the minimum device capacitance measured in the dark, usually the same in both measurements, corresponds to the series sum of the insulator and semiconductor capacitances [18,24]. The condition $d_p(t) = d_{P3HT}$ then defines the maximum width of the depletion region which occurs when the P3HT film is fully depleted. As indicated above, N_A was determined from the linear slope of the C^{-2} vs *V* plot. The relative permittivity of P3HT was assumed to be three. Other parameters such as the device area (3.14 mm^2), incident photon flux (proportional to *K*), the voltage ramp rate, γ, and the maximum voltage applied, V_f, were chosen to match experimental conditions.

In Fig. 5 we show the simulated *C–V* curves both in the dark and for illumination with photons in the range 700–400 nm. The only disposable parameter in the simulations is *K* which here we have chosen to provide a good fit to the C_{min} values observed experimentally in each of the plots in Fig. 2. The values of *K* used (Table 2) are almost identical for the 400 nm and 700 nm plots but somewhat lower for the 500 nm and 600 nm plots.

As can be seen, the resulting simulations predict the correct trend for the width of the hysteresis but in all cases overestimate the shift in V_{FB} during the reverse sweep. In the simulations, the return plots rise rapidly to the accumulation capacitance. This immediate rapid rise is not seen experimentally. Initially, the capacitance rises slowly and only when the applied voltage has decreased by about 1–2 V does the return plot become a shifted version of that seen during the forward scan. This difference in behaviour is significant since it suggests that the experimental results may be reflecting the presence of an optically-induced weak inversion layer which is not included in the model. We will return to this point in the next section.

Fig. 6 shows the simulated *C–V* plots for different light intensities but at a constant voltage ramp rate of 0.2 V/s. Values for *K* (Table 3) were now chosen to fit the experimentally observed values of C_{min} in Fig. 3. While *K* scales perfectly with I_0 for the two highest intensities, a much higher value is necessary for a good fit at the lowest intensity. Since all the measurements were made at the same wavelength (500 nm), reflection at interfaces and absorption in the ITO/SU8 layers will attenuate the light reaching the P3HT by the same factor. The higher *K* value at low intensity suggests, therefore, that electron generation and/or interface trapping rates are much higher in this case.

Table 2
Values of the parameter *K* and the zero-field quantum yield $\eta.\xi(0)$ providing the best fit to the experimentally observed C_{min} for different wavelengths in Fig. 2.

λ (nm)	I_0 (W/m^2)	*K*	Yield $\eta.\xi(0)$
700	1.03	2.6×10^8	1.9×10^{-4}
600	1.85	0.7×10^8	3.3×10^{-5}
500	1.86	0.9×10^8	5.1×10^{-5}
400	1.92	2.8×10^8	1.9×10^{-4}

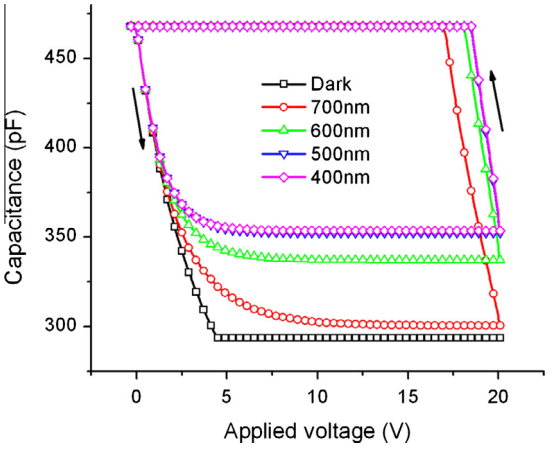

Fig. 5. Simulated *C–V* plots showing the effect of changing the wavelength of the incident light. The voltage ramp rate was 0.2 V/s. The light intensity parameter, *K*, was chosen to match the minimum capacitance for each individual plot in Fig. 2.

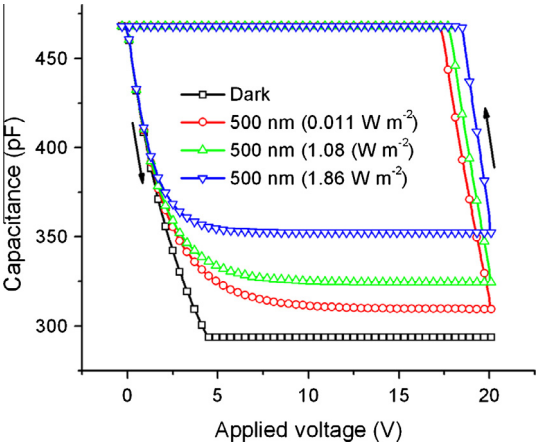

Fig. 6. Simulated *C–V* plots showing the effect of changing the light intensity parameter *K* to ensure a good match with the experimentally observed minimum capacitance. The wavelength is 500 nm and voltage ramp rate 0.2 V/s.

Table 3
Values of the parameter K and the zero-field quantum yield $\eta.\xi(0)$ providing the best fit to the experimentally observed C_{min} in Fig. 3 for different incident intensity, I_0 (λ = 500 nm).

I_0 (W/m^2)	K	$\eta.\xi(0)$
0.011	4.0×10^7	3.9×10^{-3}
1.08	5.2×10^7	5.1×10^{-5}
1.86	9.0×10^7	5.1×10^{-5}

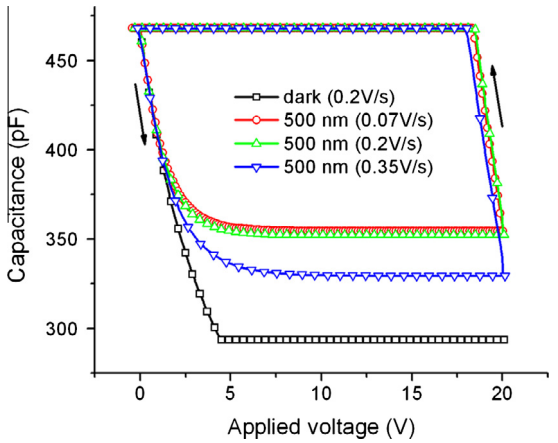

Fig. 7. Simulated C–V plots for different voltage ramp rates for 500 nm photons. The light intensity parameter, K, was chosen to fit the minimum capacitance of the individual plots observed experimentally in Fig. 4.

Table 4
Values of the parameter K and the zero-field quantum yield $\eta.\xi(0)$ providing the best fit to the experimentally observed C_{min} in Fig. 4 for different voltage ramp rates, γ (λ = 500 nm).

γ (V/s)	K	$\eta.\xi(0)$
0.07	3.3×10^7	1.9×10^{-5}
0.2	9×10^7	5.1×10^{-5}
0.35	1×10^8	5.7×10^{-5}

Finally, in Fig. 7 we simulate the effect of voltage ramp rate for illumination with 500 nm photons at constant incident power. The K values (Table 4) were chosen this time to fit C_{min} in Fig. 4. Here we see that, although the ramp rate increased by a factor five, K only increases by a factor three with only ~12% increase occurring when the ramp rate increased from 0.2 to 0.35 V/s. Nevertheless, the behaviour mirrors that found when changing the intensity – increasing the incident photon dose leads to lower values of K, suggesting either an increased recombination rate in the P3HT or that a maximum is being approached in the trapped electron population.

6. Discussion

The model developed in section 4 predicts well the general shape of the photon-assisted C–V plot – initially following the dark plot, breaking off to a minimum capacitance, C_{min}, plateau well before the semiconductor depletes fully and finally showing strong hysteresis upon reversing the voltage scan. Although appearing to be an inversion-like plateau, C_{min} has been reproduced here without the need to invoke the presence of free electrons at the semiconductor interface. The plateau occurs as a direct result of electron trapping, specifically as a result of the electron trapping rate reaching a critical value during depletion so that the term ($V(t)$–$V_{FB}(t)$) in Eq. (14) and, hence, the measured capacitance (Eq. (3)) become constant. The model also predicts the influence of experimental parameters on C_{min} albeit that the values of K, the only disposable parameter, must be adjusted to provide a good fit to the experimental data.

Eq. (11) shows that, after correcting for incident light intensity, the parameter K provides a direct measure of the conversion efficiency, $\eta.\xi(0)$, from photons to free electrons (i.e. the quantum yield) and, if the model is correct, thence to the trapped electrons density. All the other parameters in Eq. (11) are known. Values for the yield have been extracted for the various experimental conditions and are also listed in Tables 2–4.

Firstly we note that the efficiencies are low, ranging from ~2×10^{-5} to ~4×10^{-3}. It should be noted, though, that these represent zero field values. At the P3HT/SU8 interface, where the electric field is at its highest (Eq. (7)), the yield will be greater by a factor $(1 + \beta F)$. Assuming that C_{min} corresponds to a depletion region that extends 60 nm, say, into the P3HT, then the electric field at the interface is ~1×10^7 V/m, $\beta F \sim 4$ so that the electron generation rate would be increased by a factor five over the zero field value. Interestingly, over the electric field range 10^7–10^8 V/m, the quantum yield in PPV-ether [34], increased from ~10^{-5} to 10^{-3}, values similar to those extracted here and close to the range 10^{-4} to 10^{-2} quoted by Pivrikas et al. [36] for π-conjugated polymers.

Comparing Figs. 2 and 5 (Table 2), we see that the yield is higher at 400 nm than at 500 and 600 nm. This is not surprising – the efficiency factors η and $\xi(0)$ will be wavelength dependent. For example, in anthracene crystals it has been shown [30] that when photon energy decreases from 5.9 to 4.2 eV, $\xi(0)$ decreases from ~0.28 to ~0.01. Our results suggest that this downward trend continues at lower photon energies. The much lower values extracted here are probably the result of much reduced photon absorption in our thin P3HT films. The characteristic absorption length, $1/\alpha(\lambda)$, at 500 nm is ~130 nm so that less than half the incident photons will be absorbed in the depletion region even if it extends to ~60 nm. It is also possible in our case that a fraction of the electrons escaping geminate recombination may undergo recombination or trapping in the P3HT itself during transit to the interface. Some may also remain free thus contributing to the creation of an electron inversion layer at the interface.

It is not clear why the yield should be so much higher at 700 nm unless it is related to the different carrier generating mechanism at this wavelength (sub-bandgap energy).

The effects of light intensity and voltage ramp rates are complementary in that these parameters control the total photon dose, $I_0.t_f$, incident on the device during the forward sweep. For the intensity range 1.08–1.86 J/m^2 and ramp rates from 0.2 to 0.35 V/s, corresponding to a factor

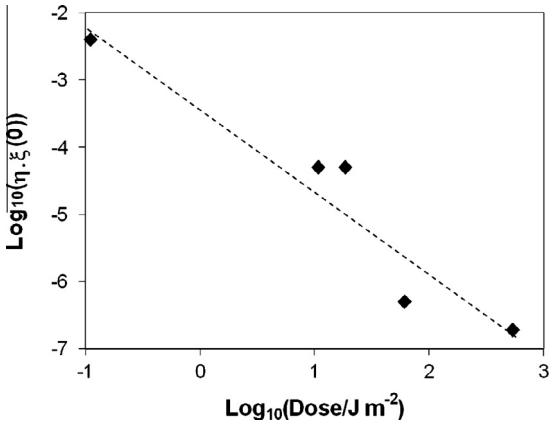

Fig. 8. Log-log plot of the extracted zero-field quantum yield, $\eta.\xi(0)$, as a function of the photon dose incident on the device during the forward voltage ramp.

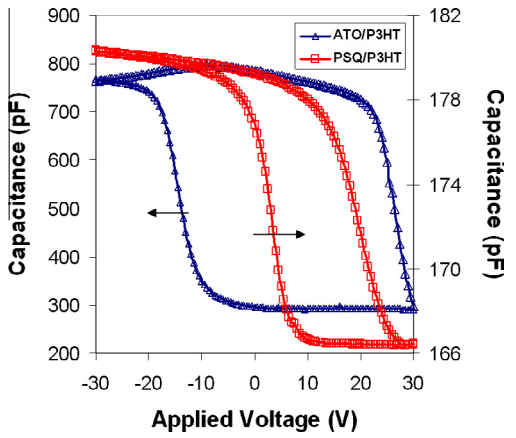

Fig. 9. *C–V* plots obtained during illumination with 500 nm light of P3HT-based MIS capacitors incorporating atomic-layer-deposited aluminium titanium dioxide (ATO) and polysilsequioxane (PSQ) as gate insulators. The PSQ results are unpublished results from the same measurement set as reference [8]. The ATO results are replotted from reference [9].

3.3 change in the incident dose, the zero-field yield, $\eta.\xi(0)$, is essentially constant at $\sim 5 \times 10^{-5}$. However, when all the results obtained for 500 nm illumination are plotted together, see Fig. 8, the data appear to follow a law of the form $\eta.\xi(0) = 3 \times 10^{-4}(I_0.t_f)^{-1.3}$ suggesting that the almost constant yield in the mid-dose range is coincidental and probably arose from experimental error.

We now return to the device response on the return voltage sweep. The simulations, based on the interface trapping of all photogenerated electrons, show an immediate and rapid rise towards the accumulation capacitance as the voltage reverses. Experimentally, the capacitance increases slowly at first before the more rapid rise sets in. Interestingly, from Fig. 9, we see that this behaviour is intermediate between those reported for organic MIS capacitors incorporating polysilsesquioxane (PSQ) [8] and atomic-layer-deposited aluminium titanium dioxide (ATO) [9] as the gate insulator. In the latter case, the initial rapid rise in capacitance observed experimentally during the reverse sweep follows closely the model prediction. In the PSQ device, on the other hand, the capacitance remains constant until the voltage decreased by about 3–4 V, only then rising towards accumulation. Such behaviour in wide bandgap inorganic semiconductors is taken as evidence for the presence of an inversion layer [2–6].

Based on our observations, we arrive at the unsurprising conclusion that the nature of the gate insulator determines the extent to which *free* electrons can accumulate at the P3HT/insulator interface. Since the response of ATO devices is consistent with our model, the capacitance minimum observed in [9] arises entirely from the shift in V_{FB} due to electron trapping. The constant capacitance observed during the initial stages of the reverse sweep for the PSQ device suggests that an inversion layer of free electrons is able to form, so long as the device remains under illumination. The intermediate response of the SU8 device suggests that there may be some free electrons present at the interface. Indeed in a separate study [37] we have shown that photogenerated free electrons do exist at the interface and can transfer along the interface from one capacitor to another as occurs in a charge coupled device.

7. Conclusions

We have undertaken an experimental study of P3HT/SU8 MIS capacitors using the photon-assisted *C–V* measurement technique. A theoretical, quasi-static model has been developed which describes the main features observed experimentally viz. the occurrence of a minimum capacitance plateau well before the device is driven into full depletion and strong hysteresis on the return voltage sweep. In the model we assumed that exciton dissociation into free electrons was governed by the Onsager model for geminate recombination so that carrier generation occurred only in the depletion region. We further assumed that all photogenerated electrons drifted to, and became trapped at, the insulator/P3HT interface. The model predicts that, at some critical point during the forward voltage ramp, the electron generation and trapping rates increase sufficiently to causes the flatband voltage, V_{FB}, to shift in the positive voltage direction at a rate equal to the applied voltage ramp rate. Consequently, no further expansion of the depletion region can occur so that the measured capacitance becomes constant.

By fitting the model to the observed capacitance minimum under various experimental conditions we show that the zero-field quantum yield, $\eta.\xi(0)$, of photogenerated electrons lies in the range 10^{-5} to $>10^{-3}$, and consistent with photocurrent measurements on other organic materials. We also show that $\eta.\xi(0)$ decreases to a constant value at the highest intensities used in this work and also decreases with total incident dose. These results show that the photon-assisted *C–V* technique provides an alternative approach to photocurrent measurements for investigating photoconductive yield in organic semiconductors. The results obtained here are relevant, therefore, to the on-going development of P3HT-based photovoltaic cells.

The model also predicts the hysteresis observed during the reverse voltage sweep. The width of the hysteresis loop is a direct measure of the density of electrons trapped at the insulator/P3HT interface, which from experiment is $\sim 10^{16}\,m^{-2}$. Consideration of the detailed shape of the *C–V* plot during the early stages of the reverse voltage sweep, has shown that the differences between the results here and those we have published previously probably arises from differences in the density of free electrons present at the insulator/P3HT interface. The technique is also useful, therefore, for investigating the interfacial properties of electrons in p-doped MIS devices.

Acknowledgements

The authors wish to record their thanks to the late Dr. T. Jenkins, Aberystwyth University, UK who provided *n-k* values from which we calculated the absorption coefficients relevant to our P3HT films. The work was partially support by Grant number EP/J021857/1 from the Engineering and Physical Sciences Research Council (UK) who also provided a PhD studentship for one of us (CPW).

References

[1] L.M. Terman, Solid State Electron. 5 (1962) 285.
[2] H.C. Casey, G.G. Fountain, R.G. Alley, B.P. Keller, S.P. DenBaars, Appl. Phys. Lett. 68 (1996) 1850.
[3] T. Hashizume, E. Alekseev, D. Pavlidis, K.S. Boutros, J. Redwing, J. Appl. Phys. 88 (2000) 1983.
[4] B. Gaffey, L.J. Guido, X.W. Wang, T.P. Ma, IEEE Trans. Electron. Dev. 48 (2001) 458.
[5] Y.Q. Wu, P.D. Ye, G.D. Wilk, Appl. Phys. Lett. 90 (2007) 143504.
[6] J. Tan, M.K. Das, J.A. Cooper, M.R. Melloch, Appl. Phys. Lett. 70 (1997) 2280.
[7] D.M. Kim, H.C. Kim, H.T. Kim, IEEE Trans. Electron Dev. 49 (2002) 526.
[8] D.M. Taylor, J.A. Drysdale, I. Torres, O. Fernández, Appl. Phys. Lett. 89 (2006) 183512.
[9] J. Lancaster, D.M. Taylor, P. Sayers, Appl. Phys. Lett. 90 (2007) 103513.
[10] O. Fernández, D.M. Taylor, J.A. Drysdale, D.M. Ellis, IEEE Trans. Dielect. El. In. 13 (2006) 1093.
[11] V. Podzorov, M.E. Gershwin, Phys. Rev. Lett. 95 (2005) 016602.
[12] Y.-Y. Noh, D.-Y. Kim, K. Yase, J. Appl. Phys. 98 (2005) 074505.
[13] Y.-Y. Noh, D.-Y. Kim, Y. Yoshida, K. Yase, B.J. Jung, E. Lim, H.K. Shim, Appl. Phys. Lett. 86 (2005) 043501.
[14] H. Sirringhaus, Adv. Mater. 21 (2009) 3859.
[15] M. Debucquoy, S. Verlaak, S. Steuel, K. Mymy, Appl. Phys. Lett. 91 (2007) 103508.
[16] I. Torres, D.M. Taylor, E. Itoh, Appl. Phys. Lett. 85 (2004) 314.
[17] C. Feng, T. Mei, X. Hu, Org. Electron. 12 (2011) 1304.
[18] E.M. Lopes, R.S. Ywata, N. Alves, F.M. Shimizu, D.M. Taylor, C.P. Watson, A.J.F. Carvalho, J.A. Giacometti, Org. Electron. 13 (2012) 2109.
[19] E.J. Meijer, A.V.G. Magnus, C.M. Hart, D.M. de Leeuw, T.M. Klapwijk, Appl. Phys. Lett. 78 (2011) 3902.
[20] E.J. Meijer, A.V.G. Magnus, B.-H. Huisman, G.W. 't Hooft, D.M. de Leeuw, T.M. Klapwijk, Synth. Metals 142 (2004) 53.
[21] G. Garcia-Belmonte, A. Munar, E.M. Barea, J. Bisquert, I. Ugarte, R. Pacios, Org. Electron. 9 (2008) 847.
[22] C.G. Fonstad, Microelectronic Devices and Circuits, International ed., McGraw-Hill, New York, 1994.
[23] I. Torres, D.M. Taylor, J. Appl. Phys. 98 (2005) 073710.
[24] D.M. Taylor, N. Alves, J. Appl. Phys. 103 (2008) 054509.
[25] M.L. Chabinyc, R.A. Street, J.E. Northrup, Appl. Phys. Lett. 90 (2007) 123508.
[26] A. Seemann, T. Sauermann, C. Lungenschmied, O. Armbruster, S. Bauer, H.-J. Egelhaaf, J. Hauch, Solar Energy 85 (2011) 1238.
[27] S.M. Sze, Physics of Semiconductor Devices, 2nd ed., Wiley-Interscience, New York, 1981.
[28] T.C. Poon, H.C. Card, J. Appl. Phys. 51 (1980) 5880.
[29] L. Onsager, Phys. Rev. 54 (1938) 554.
[30] R.H. Batt, C.L. Braun, J.F. Horning, J. Chem. Phys. 49 (1968) 1967.
[31] D.M. Pai, R.C. Enck, Phys. Rev. B 11 (1975) 5163.
[32] R.C. Hughes, Chem. Phys. Lett. 8 (1971) 403.
[33] D.M. Taylor, A.A.A. Al-Jassar, J. Phys. D: Appl. Phys. 14 (1981) 1531.
[34] S. Barth, H. Bässler, Phys. Rev. Lett. 79 (1997) 4445.
[35] V.I. Arkhipov, E.V. Emelianova, H. Bässler, Chem. Phys. Lett. 340 (2001) 517.
[36] A. Pivrikas, G. Juška, R. Österbacka, M. Westerling, M. Viliūnas, K. Arlauskas, H. Stubb, Phys. Rev. B 71 (2005) 125205.
[37] C.P. Watson, D.M. Taylor, Appl. Phys. Lett. 99 (2011) 223304.